

## **Microstructure and electro-magnetic properties of a nickel-based anti-magnetic shielding alloy**

T. Bauer<sup>1</sup>, A.B. Spierings<sup>1</sup>, K. Wegener<sup>2</sup>

<sup>1</sup> Innovation Centre Additive Manufacturing Switzerland, Inspire AG, St.Gallen, Switzerland

<sup>2</sup> Institute of machine tools and manufacturing, Inspire AG, Tannenstrasse 3, 8092 Zurich, Switzerland

### **Abstract**

Selective Laser Melting (SLM) is capable producing high performance parts e.g. for the aerospace or turbine industry. Nonetheless there is a high potential in other sectors such as in the electronic industry. For these applications, optimal properties of magnetic flux, coercive force and hysteresis are required. An isotropic microstructure is favoured - a condition hardly achieved by the SLM process. The SLM-processing window for a NiFe14Cu5Mo4 alloy is developed and basic microstructure is presented. The electro-magnetic properties are measured using a specific test bench allowing a direct comparison of the properties with a reference material. The results are discussed with a specific focus on the effect of the microstructure on the industrial usage.

Keywords: Selective Laser Melting, Additive Manufacturing, Anti-Magnetic Shielding Alloy, Magnetic properties

### **Introduction**

In the past years Additive Manufacturing and especially Selective Laser Melting (SLM) developed from a prototyping technology towards a manufacturing technology, ready to be integrated in the work flow of a traditional manufacturing environment as demonstrated by the machines of EOS [1], Additive Industries [2], or the “Factory of tomorrow”-idea of Concept Laser [3]. Furthermore SLM is known to layer wise create complex shaped parts for dominantly tooling applications, structural parts for aerospace- (Uriondo et al. [4]), turbine- (Klocke et al.[5]) and medical applications.

The SLM-process is a powder-bed based additive manufacturing technology where a focussed Nd:YAG laser source with a wavelength of 1064 nm is used to selectively melt 2-dimensional cross-sections of a 3-dimensional part. After the consolidation of a cross-section the required substrate plate is lowered, a new powder layer is applied and the scanning process starts again.

Soft magnetic materials are used in a wide range of electronic devices. Examples are stepper motors to precision positioning devices. In such applications, the typical part sizes are often suitable to the SLM build envelope. Therefore, additive manufacturing of such materials would be an interesting application.

Compared to hard magnetic materials (often called permanent magnets) soft magnetic materials offer very low hysteresis losses that occur during the change of the polarisation of the magnet as

shown by Hattendorf [6]. Furthermore the hysteresis curve can be exactly tuned towards to specific requirements for various applications through compositional changes as well as heat treatments and their resulting microstructural changes as discussed by Nunes et al. [7]. Conventional parts using soft-magnetic alloys are typically manufactured by powder metallurgical methods such as metal injection moulding which is addressed by powder injection molding international [8], sheet metal and rarely bulk material with larger wall thicknesses.

The NiFe14Cu5Mo4 material in the present study is often used for magnetic-shielding components, and is also known as MuMetall, Magnifier 7754, or RNi5. So far there have been no studies on the processing of this specific alloy by Additive Manufacturing, or specifically SLM.

Nonetheless studies on other magnetic materials have been conducted for example by Shishkovsky and Saphronov [9] who investigated peculiarities of SLM processed Permalloy and showed promising results for a successful consolidation of the material. Another paper by Zhang et al. [10] deals with in-situ formation of magnetic intermetallic compounds during processing of an alloy containing 80 % iron and 20 % nickel. They showed that the magnetic properties could be influenced by laser scanning parameters and especially by the scanning speed. It could be demonstrated that scanning velocities below 400 mm/s improved the magnetic saturation.

## **Material and Methods**

### **Raw Material**

The shielding alloy was sourced from two different vendors. Vendor “A” supplied the material from stock with a particle size between 7.5  $\mu\text{m}$  to 40.7  $\mu\text{m}$  produced with argon atomisation. In the as delivered condition the material showed a flowability not suitable for the SLM process with an optical evaluation of  $\phi = 4$  according to the scale introduced by Spierings et al. [11]. In order to improve the flowability, 0.03 wt-% of nano-scaled silica has been added resulting in a rating of  $\phi = 1.5$  enabling a reliable recoating process. The second supplier Vendor “B” specifically atomized a material with the same specification as the material from vendor A. Due to a coarser particle size specification of vendor “B” ranging from 15  $\mu\text{m}$  to 45  $\mu\text{m}$  the flowability was improved over that of vendor “A” with an as delivered flowability of  $\phi = 2.5$ . The optical comparison of the powder can be seen in Figure 1 as well as in Figure 2.

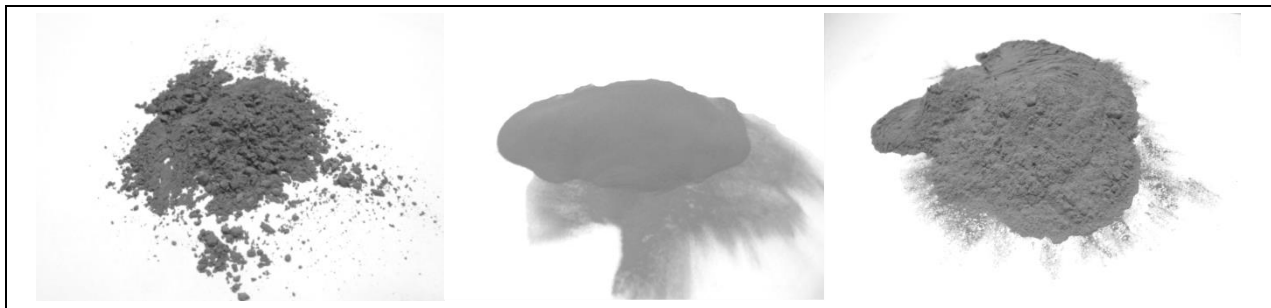


**Figure 1: Optical comparison of Vendor “A” in as delivered condition (left), with added nano-silica (middle) and Vendor “B” (right)**

The comparison of the SEM images in Figure 2 clearly displays the increased amount of fine particles of vendor “A” and the more regular, spherical shape of the particles. This leads to the insufficient flowability in the as-delivered condition. The custom gas atomized powder of vendor “B” exhibits coarser, odd shaped particles with more satellites.

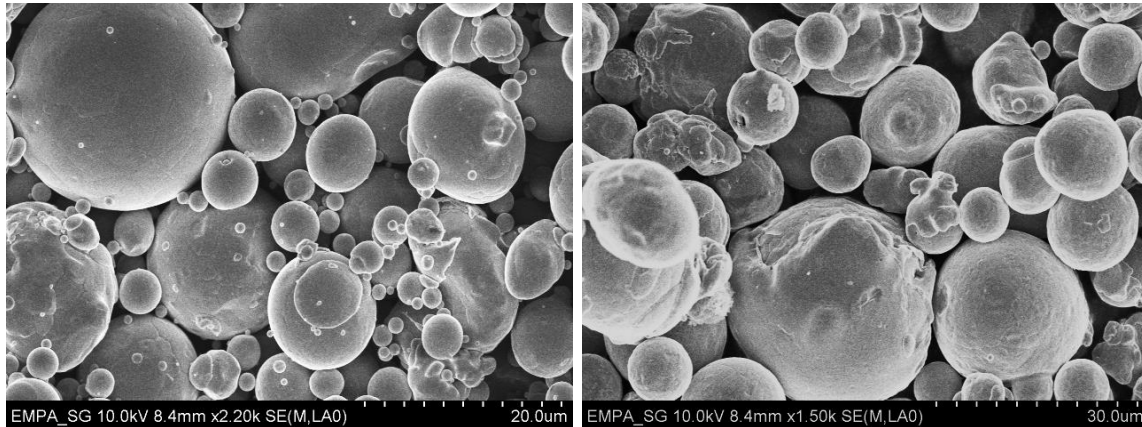


**Figure 2: SEM images of gas atomized powder of vendor "A" without added nano-silica (left) and vendor "B" (right)**

The chemical composition of the vendor “B” material was adjusted to fit the chemical composition of vendor “A” allowing a better comparability and to test the reproducibility of the results under near industry conditions with varying batches. The results of the chemical analysis are shown in Table 1, and were measured using a SPECTROMAXx Optical Emission Spectroscopy (OES) device.

**Table 1: Chemical composition of NiFe4Cu5Mo4 measured by Optical Emission Spectroscopy**

	Ni	Fe	Cu	Mo	Sn	Ta	C	Si	P	S	Rest
	wt-%										
<b>Nominal</b>	Bal.	14	5	4	-	-	-	-	-	-	-
<b>Vendor “A”</b>	Bal.	16.650	5.540	3.420	0.802	0.724	0.015	0.031	0.002	0.001	0.236
<b>Vendor “B”</b>	Bal.	16.650	5.240	3.670	0.821	0.664	0.031	0.034	0.002	0.006	0.175

The composition of both material variants are similar, and are within the measurement deviation of the used device. Nonetheless it is clear that OES has sensitivity limits especially for light elements such as silicon or nitrogen that can have significant influence on the materials processing behaviour for SLM which has been demonstrated by Engeli et al. [12] for the nickel-based alloy Inconel 738LC.

### Experimental setup

During the parameter study a Concept Laser M1 “CL-M1” (focus spot diameter 120 μm) and M2 “CL-M2” (focus spot diameter 90 μm) have been used in order to investigate the influence of the different laser intensities to the material. Both machines are equipped with a similar recoating system, in order to create similar powder bed conditions. A wide range of SLM-processing

parameters have been applied to determine possible parameter combinations for various requirements such as productivity, low surface roughness or high material density. The selected parameters and their ranges are shown in

Table 2 for both machines. As a measure to evaluate the energy input during the melting process the volume energy density  $E_{vol}$  (1) is used which incorporates the main influencing process parameters laser power  $P$  (W), scan velocity  $v_s$  (mm/s), layer thickness  $t$  (mm) as well as the hatch distance  $d$  (mm) :

$$E_{vol} = \frac{P}{v_s \cdot t \cdot d} \quad (1)$$

**Table 2: Parameter range used for SLM of NiFe14Cu5Mo4**

	Layer thickness $t$ ( $\mu\text{m}$ )	Scan speed $v_s$ ( $\text{mm/s}$ )	Hatch distance $d$ ( $\mu\text{m}$ )	Volume energy density ( $\text{J/mm}^3$ )
Concept Laser M1 (P=100 W)	30	150 – 300	95 – 110	98 – 228
Concept Laser M2 (P=200 W)		450 – 1350	75 – 105	53 – 186

10x10x10 mm<sup>3</sup> test cubes were produced using a meander like scanning pattern shown in Figure 3 that alternated by 90° between each layer, which reproduces the production pattern used by Concept Laser systems. Furthermore it is known that the rotation of the scanning pattern leads to an increase of consolidated material density compared to a repeated scan as demonstrated by Kruth et al. [13]. During the optimisation of the build process two scan strategies have been investigated: The above mentioned standard scan strategy with a single scan of each layer and a second with re-scan of the same layer using less energy per scan.

Archimedes method was used in order to determine the relative density using Acetone as the measurement fluid in accordance with the recommendation of Spierings et al. [14]. The reference density was set to 8.72 g/cm<sup>3</sup> as reported on the material data sheet of vendor “A” batch.

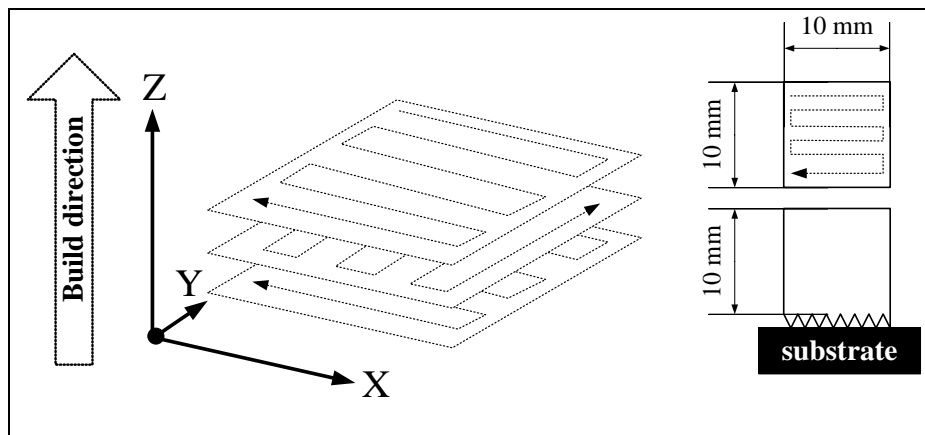


**Figure 3: Alternating scan pattern (left) and sample dimensions for density measurements (right)**

The cube specimens were cross sectioned to expose planar surfaces parallel (xz-plane) as well as perpendicular (to expose the xy-plane) to the build direction. Samples were prepared using standard metallographic techniques and a final polish was applied using colloidal silica. The samples were immersion etched using Kalling-2 reagent. Optical microscopy was carried out on a Keyence VHX-1000.

The hysteresis measurement was conducted in accordance with IEC/DIN EN 60404 [15] employing a ring shaped sample with an inner diameter  $d_i = 22$  mm, outer diameter  $d_a = 30$  mm and a thickness  $t = 4$  mm. Simplified the hysteresis loop for d.c. soft magnetic materials is recorded using an experimental setup with a field generator and coil (see Figure 4, “H”) that can log the magnetising current with an accuracy of  $\pm 0.5$  % as well as a magnetic flux measurement coil and device (see Figure 4, “B”) with an accuracy better than  $\pm 1$  %. Both field generator coil and flux measurement coil had  $n = 10$  turns (Figure 4). For each of the investigated scan strategies (standard and re-scan) a vertical (ring upright) and horizontal sample (ring parallel to substrate) were built and a so called “block support” was used to support the overhanging structures (Figure 4, left). After the support removal a steel blasting operation (operating pressure 4.5 bar) was applied on all samples.

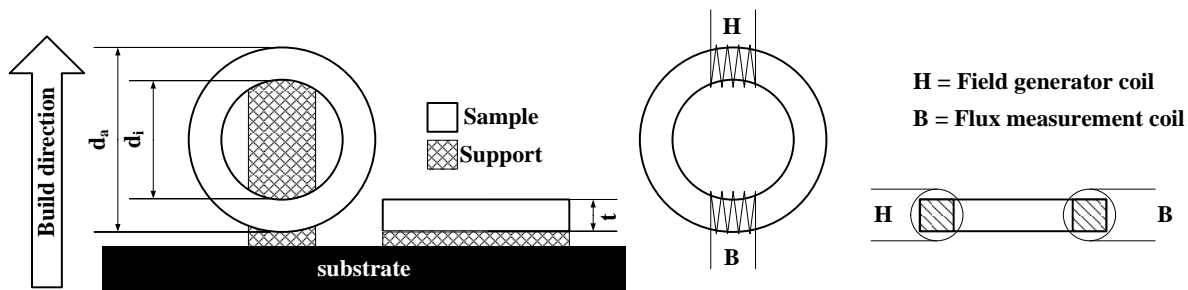


**Figure 4: Orientation of the ring samples on the substrate (left) and placement of the coils in reference of the build direction (right)**

## Results and discussion

The first trials in this study were conducted with material from vendor “A” on the Concept Laser M1 SLM system and exhibited good processing characteristics over a wide range of build parameters. The resulting parameter set was narrowed down to a very confined space as one of the key requirements was to achieve the smallest possible size of build errors, hence a low level of porosity (keyhole as well as interlayer errors) and no cracking. There was no cracking encountered during the processing of the material of vendor “A”. The processing window is very narrow between a significant number of interlayer bonding errors and key-hole welding induced porosity which can be seen in Figure 5. Therefore a parameter with a volume energy density between  $190 \text{ J/mm}^3$  and  $210 \text{ J/mm}^3$  is chosen in order to achieve acceptable material integrity.

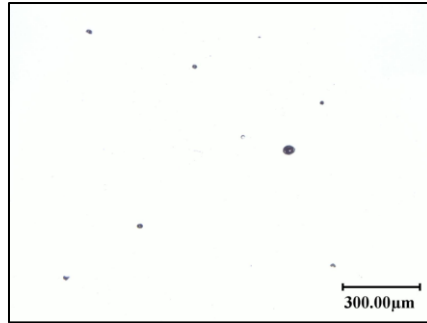


**Figure 5: Material of Vendor "A" processed on a CL-M1 exhibiting key hole porosity**

Based on initial results, and in order to analyse the effect of an increased laser intensity a comparative study of two powders on the CL-M2 machine was performed. During those trials the material of vendor "B" was introduced in order to analyse the effects of powder differences (particle size distribution, specific composition and amount of residual elements such as Si, O, N).

The results in Table 3 display that powder "A" results in significantly better material integrity, hence lower pore level, and almost no cracking. The material of vendor "B" exhibits a large amount of cracks and pores that will lead to higher magnetic losses compared to material built with powder A, as well as a decrease in mechanical properties.

**Table 3: Comparison of consolidated material by Concept Laser M2 of vendor A and vendor B**

	xz-plane	etched
Vendor A		
Vendor B		

A clear reason for the cracking issue of powder B is not yet elaborated. However, a possible reason could be the variation of the silicon content. Due to the lack of flowability of vendor “A” powder nano-scaled silica was mixed into the powder, in order to gain a sufficient flowability for the SLM process. In the development period a concentration test was conducted in order to define upper and lower limit of the flowability enhancer addition. An addition of nano-scaled silica between 0.03 wt.-% and 0.05 wt.-% was tested. Additions above 0.04 wt.-% of silica were sufficient to cause minor unsystematic cracking. As additions of 0.03 wt.-% silica were sufficient to increase the flowability significant the amount of silica should be limited to 0.03 wt.% for this specific alloy. This observation is similar to the findings stated in the publication of Engeli et al. [12] where low additions of silicon caused severe cracking in the consolidated material. Furthermore Davies et al. [16] state the hot-cracking susceptibility can be increased with a rising content of silicon.

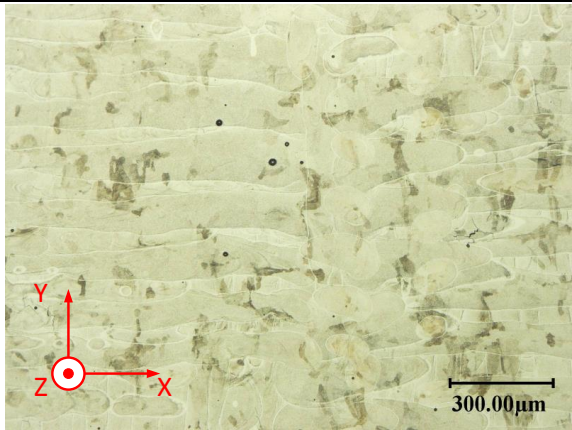
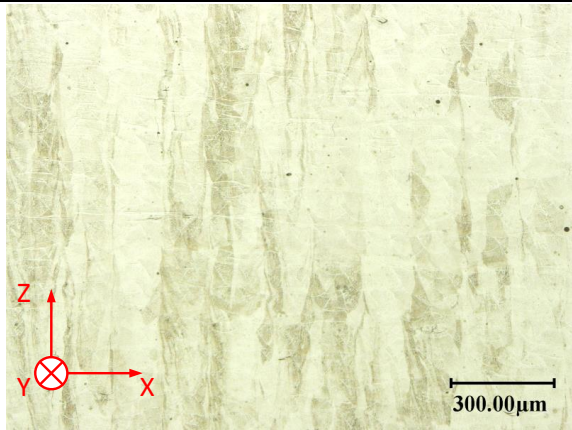
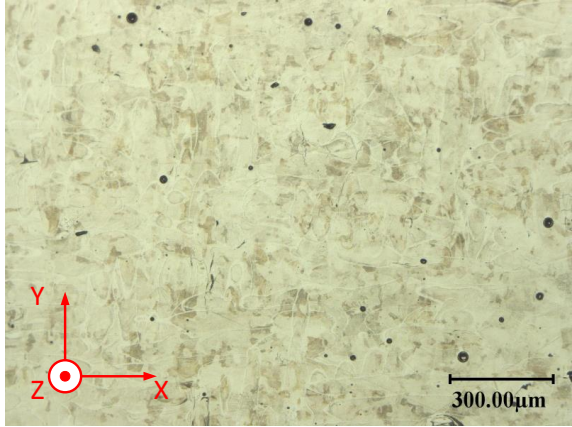
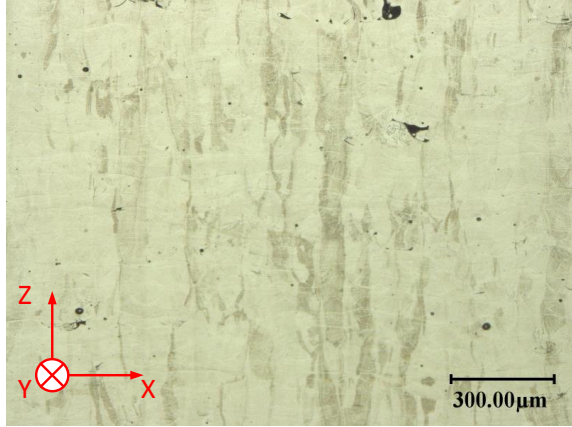
The batch of vendor “A” material was then successfully consolidated with volume energy densities over  $140 \text{ J/mm}^3$  on the Concept Laser M2 system with the restriction that only spherical pores are tolerable.

#### Scan strategy optimisation

The high energy input needed for full consolidation results in various effects during the consolidation process, such as increased surface roughness in overhanging sections, an SLM characteristic microstructure with columnar grains oriented predominately in the build (z) – direction as well as in general a limitation of the geometric complexity due to part-distortion. Therefore it is essential to analyse the influence of different scan strategies to find optimal results.

Kruth et al. [13] described a scan strategy involving remelting of the same layer in order to create a smoother surface for recoating as well as remelting of intrinsic porosity. During the present study the major aim of this scan strategy modification was to interrupt the grain growth in the build direction. The limitation of grain growth was successfully implemented during the processing of Haynes 230 demonstrated by Bauer et al. [17]. Therefore the strategy of double scanning of a single layer was applied, where both scans were performed with half the volume energy density of the standard scan strategy. The qualitative comparison of the results of the test cubes can be seen in Table 4.

**Table 4: Comparison of etched micrographs of standard scan and re-scan**

	xy-plane	xz-plane
Standard Scan		
Re-scan		

During the analysis of the xy-plane micrographs it is clear that the weld pool width is significantly increased with the standard scan strategy over the re-scan strategy. As a result of the constant hatch distance the ratio of remolten material to the overall melt pool dimension decreases. This impression is emphasized in the micrographs of the xz-plane that exhibit a dependency between melt pool width and width of the grains. However, an effect on the grain growth in z-direction cannot be clearly identified as the x-z-planes micrographs of both scan strategies show similar structures.

#### Microstructure on part level

The SLM-process has numerous thermal boundary conditions influencing residual stresses, distortion, and finally the microstructure of the part. This can lead to a significant anisotropy of the mechanical properties of around 15 % with regard to horizontal and vertical build orientation. Therefore it was necessary to optimize the part orientation and related support type selection and -placement, and to analyse their impact on the microstructure as well as the final magnetic properties after the build job. Table 5 gives an indication of the microstructure of three different sections in the upper quarter of the vertical built ring samples. It is clear that despite the general microstructural changes described above the effect of the geometry in combination with the scanning strategy is not significant in areas which have sufficient heat conduction towards the



substrate, which is the case near the substrate (left section) as well as near the supported areas (top section).

**Table 5: Comparison of etched micrographs of ring samples using standard scan and re-scan strategy (arrows indicating the grain growth direction)**

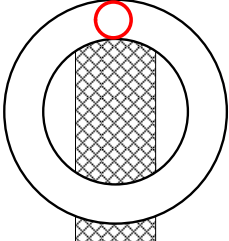


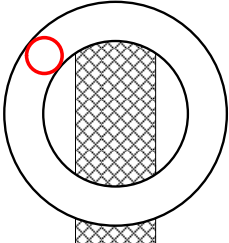
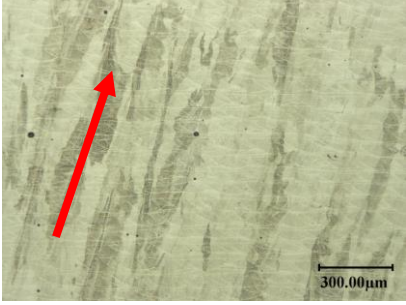
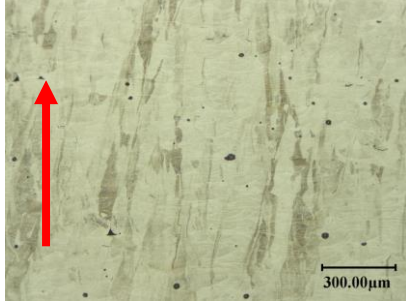
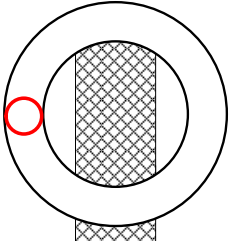
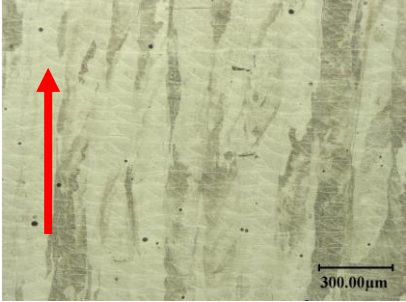

Ring position	Standard scan	Re-scan
 <p style="text-align: center;">top</p>		
 <p style="text-align: center;">middle</p>		
 <p style="text-align: center;">left</p>		

Table 5 shows that with the standard scan strategy the grain growth follows the direction of the temperature gradient, which is the direction opposite of the heat flow. Therefore the main grain orientation in the middle position is tilted  $\approx 20^\circ$  from the vertical axis. In contrast to that the stepwise heat input during the re-scan strategy still shows a nearly vertical grain growth. This results in a homogeneous grain orientation and microstructure throughout the whole part, whereas the standard scan strategy results in effects from the geometry on the microstructure due to the heat conduction conditions.

Next to these positive effects of the re-scan strategy, a negative effect is the slight reduction of the material density by about 0.5% (standard scan strategy  $99.96 \pm 0.03 \%$ , re-scan strategy  $99.46 \pm 0.09 \%$ ).

## Magnetic testing

The results of the magnetic testing are presented in Table 6 and Table 7 displaying the dependency of coercive force and magnetic saturation in relation to the build direction as well as the scan strategy.

**Table 6: Absolute and relative difference of coercive force and magnetic saturation in dependence of the build direction**

	Horizontal		Vertical	
	Coercive force	Saturation	Coercive force	Saturation
	Hc [A/m]	Ms [T]	Hc [A/m]	Ms [T]
<b>Standard Scan</b>	29.4	0.330	25.1	0.290
<b>Re-scan</b>	33.8	0.270	32.0	0.270
<b>Abs. Difference</b>	4.4	0.060	6.9	0.020
<b>Rel. Difference</b>	<b>13.0%</b>	<b>22.2%</b>	<b>27.5%</b>	<b>6.9%</b>

The values of the coercive force as well as the magnetic saturation indicate a better magnetic performance of the standard scan strategy compared to the re-scan strategy. The increased performance is probably caused by the decreased porosity as well as the slightly coarser grain structure of the standard-scanned material. The largest relative difference of 27.5 % (absolute 6.9 A/m) between the scan strategies can be encountered at the coercive force at the vertically built samples whereas the horizontal samples only show a difference of 13.0 %. The magnetic saturation exhibits an opposite trend – the relative difference of the vertical samples is much smaller (6.9 %) than the ones of the horizontally built samples (22.2 %).

**Table 7: Results of hysteresis measurement for standard and re-scan strategy in both horizontal and vertical build direction**

	Standard scan		Re-scan	
	Coercive force	Saturation	Coercive force	Saturation
	Hc [A/m]	Ms [T]	Hc [A/m]	Ms [T]
<b>Horizontal</b>	29.4	0.330	33.8	0.270
<b>Vertical</b>	25.1	0.290	32.0	0.270
<b>Abs. Difference</b>	4.3	0.040	1.8	0.000
<b>Rel. Difference</b>	<b>17.1%</b>	<b>13.8%</b>	<b>5.6%</b>	<b>0.0%</b>

Obviously the standard scan strategy causes anisotropy in both the coercive force (17.1 % rel. difference) and the magnetic saturation (13.8 % rel. difference). In contrast to this, the re-scan strategy causes only 5.6 % relative difference respectively no difference in magnetic saturation. It can be stated that the re-scan strategy leads to a nearly identical microstructure within the whole part providing for a homogeneous baseline for any following post-treatments.

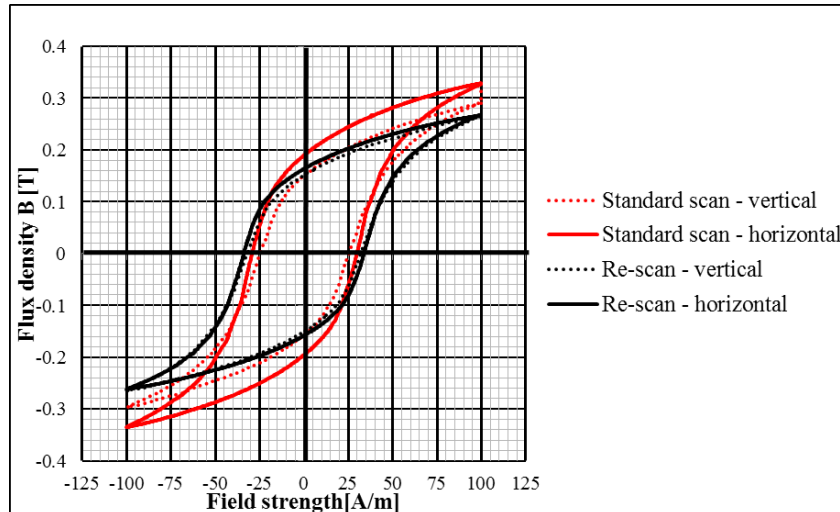


**Figure 6: Hysteresis curve (Field strength vs. flux density) of standard scanned and re-scanned material in both vertical and horizontal build direction**

The analysis of Figure 6 leads to the identical result – the hysteresis loop of the re-scanned material is almost identical whereas the standard scans show a clear deviation from each other.

Nonetheless the as-built condition - independent of the scan strategy - does not reach the magnetic properties of standard wrought-material with a coercive force of 15 A/m as well as a magnetic saturation of 0.8 T according to Vacuumschmelze GmbH [18]. This might be a result of the much finer microstructure or the increased defect number and size of the SLM built material.

### **Conclusion and outlook**

NiFe14Cu5Mo4 powder can successfully be consolidated by Selective Laser Melting if the chemical composition is precisely controlled. However, it can be assumed that minor compositional changes of residual elements (Si, O, N) can potentially lead to severe cracking as demonstrated by the test with an increased concentration of nm-scaled silica. A volume energy density over 140 J/mm<sup>3</sup> is needed in order to achieve almost fully dense material with only minor spherical pores on a Concept Laser M2 system.

The material shows a SLM typical microstructure with in z-direction elongated grains. The grain dimensions can be controlled to a certain extend by the scanning strategy used. Furthermore it was displayed that the re-scan strategy allows for nearly isotropic magnetic properties whereas the standard scan strategy leads to geometry dependent anisotropic properties. Nonetheless the material does not fulfil the values set by fully heat treated wrought material in the as-built condition.

A detailed investigation of the cracking phenomena and additional microstructural characterisation will be performed in order to build up the basic knowledge needed to provide design-, build and post treatment guidelines for this magnetic alloy. Additional heat treatment tests will be performed to accommodate the different scan strategies as well as to determine the final material properties in the finished product.

## Literature

1. EOS Systemdatenblatt EOS M400. 2016, EOS GmbH: Krailling.
2. N.N. *Introduction to Metal Fab1*. 2016 [cited 2016; Available from: <http://additiveindustries.com/Industrial-am-systems/Metalfab1>].
3. N.N. *Factory of tomorrow*. 2016 [cited 2016; Available from: <http://www.concept-laser.de/am-factory-of-tomorrow.html>].
4. Uriondo, A., Esperon-Miguez, M., and Perinpanayagam, S., *The present and future of additive manufacturing in the aerospace sector: A review of important aspects*. Proceedings of the Institution of Mechanical Engineers, Part G: Journal of Aerospace Engineering, 2015.
5. Klocke, F., Klink, A., Veselovac, D., Aspinwall, D.K., Soo, S.L., Schmidt, M., Schilp, J., Levy, G., and Kruth, J.-P., *Turbomachinery component manufacture by application of electrochemical, electro-physical and photonic processes*. CIRP Annals - Manufacturing Technology, 2014. **63**(2): p. 703-726.
6. Hattendorf, H., *Weichmagnetische Werkstoffe auf Ni-Fe-Basis*, in *VDM Report2014*, VDM Metals GmbH: Werdohl. p. 48.
7. Nunes, R., Adams, J.H., Ammons, M., Avery, H.S., Barnhurst, R.J., Bean, J.C., and Beaudry, B.J., *Nonferrous Alloys and Special-Purpose Materials* ASM Handbook Properties and Selection Vol. 2. 1990, Materials Park (OH): ASM International.
8. N.N. *High density Metal Injection Moulding (MIM) offers potential for soft magnetic applications*. 2009 [cited 2016; Available from: <http://www.pim-international.com/high-density-metal-injection-moulding-mim-offers-potential-for-soft-magnetic-applications/>].
9. Shishkovsky, I. and Saphronov, V., *Peculiarities of selective laser melting process for permalloy powder*. Materials Letters, 2016. **171**: p. 208-211.
10. Zhang, B., Fenineche, N.-E., Liao, H., and Coddet, C., *Magnetic properties of in-situ synthesized FeNi<sub>3</sub> by selective laser melting Fe-80%Ni powders*. Journal of Magnetism and Magnetic Materials, 2013. **336**: p. 49-54.
11. Spierings, A.B., Voegtlin, M., Bauer, T., and Wegener, K., *Powder flowability characterisation methodology for powder-bed-based metal additive manufacturing*. Progress in Additive Manufacturing, 2015.
12. Engeli, R., Etter, T., Geiger, F., Stankowski, A., and Wegener, K. *Effect of Si on the SLM processability of IN738LC*. in *Solid Freeform Fabrication Symposium*. 2015. Austin (TX): University of Texas.
13. Kruth, J.P., Badrossamay, M., Yasa, E., Deckers, J., Thijs, L., and Van Humbeeck, J. *Part and material properties in selective laser melting of metals*. in *16th International Symposium on Electromachining*. 2010. Shanghai, China.
14. Spierings, A.B., Schneider, M., and Eggenberger, R., *Comparison of density measurement techniques for additive manufactured metallic parts*. Rapid Prototyping Journal, 2011. **17**(5): p. 380-386.
15. DIN. 60404-4: Magnetic Materials. 2009.
16. Davies, J., *Nickel, Cobalt and Their Alloys*. ASM Speciality Handbook ed. J. Davies. 2000, Materials Park, OH: ASM International.
17. Bauer, T., Dawson, K., Spierings, A.B., and Wegener, K. *Microstructure and mechanical characterisation of SLM processed Haynes® 230®*. in *Solid Freeform Symposium*. 2015. Austin (TX), USA.
18. *Weichmagnetische Werkstoffe und Halbzeuge*. 2002, Vacuumschmelze GmbH & Co. KG: Hanau.